INTERNATIONAL JOURNAL FOR NUMERICAL METHODS IN FLUIDS
Int. J. Numer. Meth. Fluids 2004; **44**:885–903 (DOI: 10.1002/fld.686)

Effect of corner angle on convection enhancement in wavy ducts with trapezoidal cross-sections

S. Savino, G. Comini*,† and C. Nonino

Dipartimento di Energetica e Macchine, Università degli Studi di Udine, Via delle Scienze 208, 33100 Udine, Italy

SUMMARY

The effect of corner angle variations on pressure drop and heat transfer characteristics is investigated in the fully developed region of wavy ducts with trapezoidal cross-sections. The resulting enhancement of convection, with respect to corresponding straight ducts, can be attributed to the formation of longitudinal vortices close to the two parallel surfaces. Numerical simulations show that Nusselt numbers and friction factors increase with the decrease of corner angle from 90 to 60°, before levelling out around 60°. Nusselt numbers and friction factors also increase with the Reynolds number, and the slopes of their representative curves increase above a critical value of the Reynolds number because of the onset of time-periodic flow oscillations. Copyright © 2004 John Wiley & Sons, Ltd.

KEY WORDS: wavy trapezoidal channels; convection enhancement; numerical simulations; longitudinal vortices; transverse vortices, time-periodic flow oscillations

1. INTRODUCTION

Ducts with trapezoidal cross-sections are often found in compact heat exchangers, recuperators, regenerators, and cooling systems for gas turbines and electronic modules. Exhaustive literature reviews of forced convection in straight ducts with trapezoidal cross-sections can be found in References [1, pp. 256–259; 2, pp. 3.68–3.70; 3] for laminar flow conditions, and in Reference [4, p. 106] for turbulent flow conditions. Numerical results for three-dimensional laminar flow and heat transfer in the entrance region of straight trapezoidal ducts are illustrated in Reference [5]. Numerical results for fully developed turbulent flows in straight trapezoidal ducts have been presented in an early numerical study of a section with a 75° corner angle [6], and in a more recent analysis related to the accuracy and reliability of turbulence models [7].

In the past few years, the tendency towards miniaturization of heat transfer equipment and the need to reduce noise emissions have directed much research interest towards the en-

*Correspondence to: G. Comini, Dipartimento di Energetica e Macchine, Università degli Studi di Udine, Via delle Scienze 208, 33100 Udine, Italy.
†E-mail: gianni.comini@uniud.it
http://www.dem.uniud.it/prof-comini/comini.htm

Received 21 June 2003
Accepted 13 October 2003

hancement of convection in low Reynolds number flows. Among the geometries that present convection-enhancing irregularities, wavy ducts are frequently employed for their simplicity. In wavy ducts with trapezoidal cross-sections, two sides remain parallel over the whole length, while the angled sides are periodically displaced to form a wavy surface. In spatially periodic ducts, also the flow and the dimensionless temperature fields tend to repeat themselves in a cyclic manner, attaining a fully developed character after a short distance from the entrance. In these fully developed regions, wall corrugations prevent the continuous growth of velocity and thermal boundary layers generating transverse and longitudinal vortices (see, for example, Reference [8]). A steady flow model for laminar forced convection in the fully developed region of wavy ducts with trapezoidal cross-sections has been proposed in Reference [9] where some numerical results, obtained by a finite volume method, have also been illustrated. The same model has then been used to investigate the influence of space ratio (average height H over length L of a corrugation cycle), corrugation angle β, and corner angle γ [10]. Computations have been performed with uniform temperature boundary conditions, for Reynolds numbers in the range $75 \leqslant Re \leqslant 2000$ and for a Prandtl number $Pr = 0.72$. It has thus been found that convection is strongly enhanced by increasing the corrugation angle β from 15 to 28°, and only slightly enhanced by increasing the space ratio H/L from 0.065 to 0.13 and decreasing the corner angles γ from 60 to 45°. In all the geometries investigated, both convection and pressure losses increase with the Reynolds number [10]. In accordance with the literature (see, for example, Reference [8]), pressure drop penalties have been attributed to secondary flows associated with longitudinal vortices and to the recirculating regions established as the flow separates from the duct walls [10]. On the contrary, convection enhancements have been attributed only to secondary flows that move the fluid from the walls to the centre [10]. In fact, because of the steady model adopted in Reference [10], no time-periodic oscillations of transverse vortices could have been detected (and transverse vortices that remain steady obstruct the main flow without enhancing convection). However, in actual flows through wavy ducts the onset of self-sustained oscillations occurs at a Reynolds number above a critical value Re_{cr} and precedes the transition to turbulence [8]. When the flow and temperature fields become unsteady, transverse vortices travel from upstream to downstream and vice versa, washing the angled duct walls and moving the fluid from these walls to the centre.

The aim of this paper is to model laminar forced convection in wavy ducts with trapezoidal cross-sections, using a finite element approach that accounts for the time-dependent physics of the flow. We will consider fully developed convection of air ($Pr = 0.72$) with flows in the laminar regime, both below and above the critical value of the Reynolds number. The approach adopted here has been originally proposed in Reference [11] and has been recently used to investigate pressure drop and heat transfer characteristics in fully developed regions of wavy ducts [12, 13]. In Reference [12] the influence of space ratio H/L and corrugation angle β has been investigated in two-dimensional wavy channels. In all the situations considered, it has been found that friction factors are much higher in wavy than in straight channels. On the contrary, significant improvements of average Nusselt numbers have been obtained only for Reynolds number above Re_{cr}. For $Re > Re_{cr}$ it has been found that friction factors and Nusselt numbers increase with both β and H/L, at least until the space ratio is kept within reasonable limits. In fact increasing the space ratio beyond a certain limit, while maintaining constant the corrugation angle, makes the flow passage similar to a plain, albeit rough, channel [12]. In Reference [13] the influence of the cross-sectional aspect ratio (width W over height H of the duct) has been investigated in wavy channels with rectangular cross-sections. It has thus

been found that both Nusselt numbers and friction factors increase with decreasing aspect ratios.

Convection enhancement induced by the increase of H/L and β, and the decrease of W/H have been repeatedly confirmed through experimental measurements in three-dimensional wavy ducts with rectangular cross-sections (see, for example, References [14–17]). Since rectangular ducts can be viewed as a particular class of trapezoidal ducts with a corner angle $\gamma = 90°$, it can be assumed that the increase of H/L and β, and the decrease of W/H enhance convection also in trapezoidal ducts. On the other hand, corner angle variations are expected to significantly affect Nusselt numbers and friction factors by bringing about changes of intensity and structure in longitudinal vortices. Consequently, this paper investigates the effect of corner angle variations on laminar forced convection in wavy trapezoidal ducts, both below and above the critical Reynolds number.

2. STATEMENT OF THE PROBLEM

The duct geometry is illustrated in Figure 1. The representation at the top is drawn to scale and the average height H is measured in a vertical direction, while the width W is measured in a horizontal direction. A counterclockwise 90° rotation of wavy trapezoidal ducts, favoured in References [9, 10], improves the rendering of three-dimensional representations. After this rotation, adopted in the remaining representations of Figure 1, readability is certainly improved but the W and H symbols end up in an unusual position. However, this notation has been maintained since in most of the literature on wavy ducts the width W is measured in a direction orthogonal to the plane where the waviness develops [12–17].

According to Figure 1, the duct geometry is completely specified by the cycle length L, measured in the x direction, the average height H, measured in the y direction, the width W measured in the z direction, the corrugation angle β and the corner angle γ. The duct is infinitely long in the x direction, and is made up of an infinite series of identical corrugation cycles. After a short distance from the entrance, the flow and the dimensionless thermal fields repeat themselves from cycle to cycle, attaining a fully developed character. These repetitive fields allow the limitation of the analysis to a single cycle, such as the one enclosed by the periodic boundaries S_1 and S_3. In the present case, however, the additional anti-symmetric periodicity of the boundary conditions between S_1 and S_2 allows the limitation of the analysis to a single module (half-cycle).

2.1. Flow and temperature fields

Assuming the thermophysical properties of the fluid to be constant and the flow to be laminar, the governing equations are the standard Navier–Stokes equations. They can be written as

$$\frac{\partial \mathbf{v}}{\partial \vartheta} + \mathbf{v} \cdot \nabla \mathbf{v} = \nu \nabla^2 \mathbf{v} - \frac{1}{\rho} \nabla p \tag{1}$$

$$\nabla \cdot \mathbf{v} = 0 \tag{2}$$

In the above equations, $\mathbf{v} \equiv (u, v, w)$ is the velocity vector, $\nabla \equiv (\partial/\partial x, \partial/\partial y, \partial/\partial z)$ is the gradient operator, $\nabla^2 \equiv \nabla \cdot \nabla$ is the Laplacian operator, ϑ is the time, ν is the kinematic viscosity,

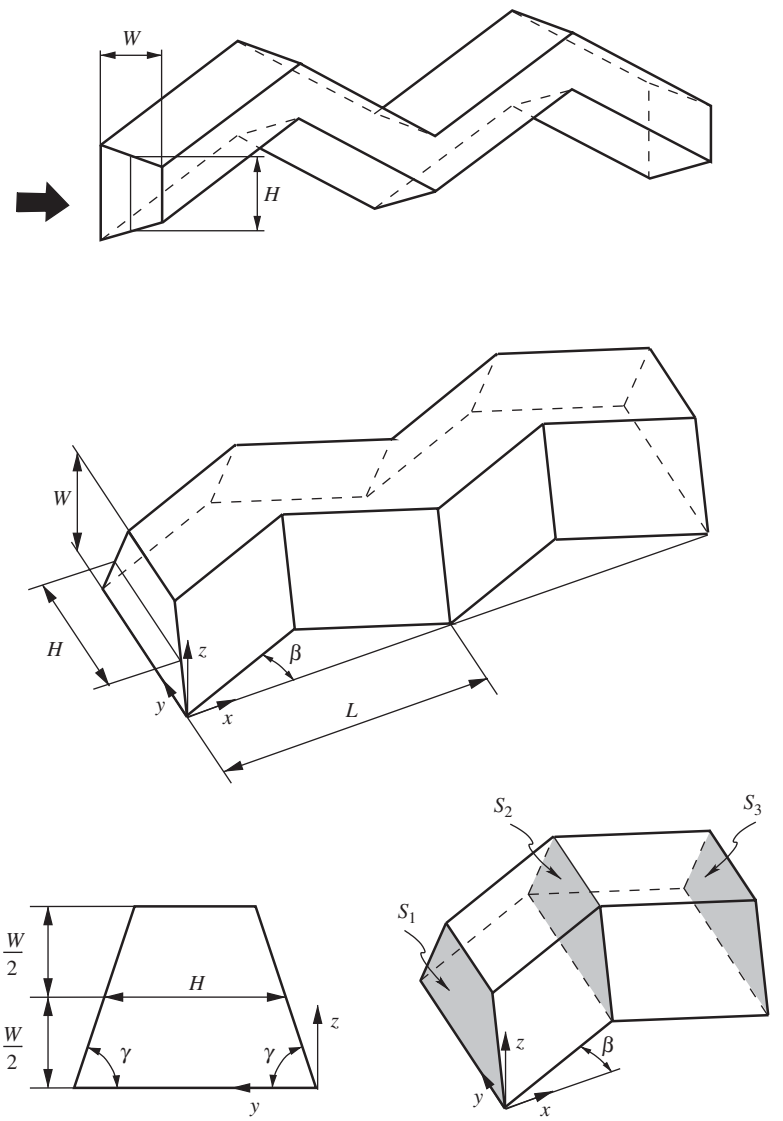

Figure 1. Wavy channels with a trapezoidal cross-section: three-dimensional view drawn to scale (top), schematic representation of two corrugation cycles after a 90° counterclockwise rotation (middle), cross-section of the duct and computational cell (bottom).

ρ is the density and p is the deviation from the hydrostatic pressure. In the absence of volumetric heating, and neglecting the effects of viscous dissipation, the energy equation can be written as

$$\frac{\partial t}{\partial \vartheta} + \mathbf{v} \cdot \nabla t = a \nabla^2 t \tag{3}$$

where a is the thermal diffusivity.

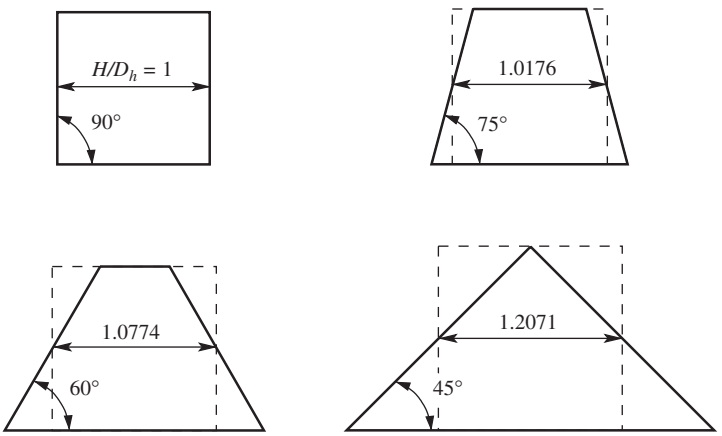

Figure 2. Cross-sectional shapes drawn to scale.

In periodic fully developed flows, the pressure p can be expressed by the sum of a linear term, accounting for the mean pressure gradient, and a residual term that behaves in a periodic manner (see, for example, References [11, 18]). Thus, for the situation illustrated in Figure 1, the pressure can be estimated as

$$p = -\alpha x + \tilde{p} \tag{4}$$

where α is a constant representing the mean pressure gradient in the main flow direction x, and $\tilde{p}$ is the periodic component. The anti-symmetric periodicity between boundaries S_1 and S_2 yields the condition

$$\tilde{p}(L/2, y'', z) = \tilde{p}(0, y', z) \tag{5}$$

where y' is the distance from the angled surface on the right, measured in the positive horizontal direction y at co-ordinates $x = 0$ and z, while y'' is the distance from the angled surface on the left, measured in the negative horizontal direction $-y$ at co-ordinates $x = L/2$ and at the same z.

Appropriate conditions must be specified at wall and anti-periodic boundaries. At wall boundaries, the no-slip condition holds good

$$u = v = w = 0 \tag{6}$$

while the anti-symmetric periodicity between boundaries S_1 and S_2 leads to the conditions

$$\begin{aligned} u(L/2, y'', z) &= u(0, y', z) \\ v(L/2, y'', z) &= -v(0, y', z) \\ w(L/2, y'', z) &= w(0, y', z) \end{aligned} \tag{7}$$

Conditions (7) do not specify any inflow velocity field. Thus the pressure gradient α must be adjusted iteratively until the desired value of the average velocity

$$\bar{u} = \frac{1}{S'} \int_{S'} \mathbf{v} \cdot \mathbf{n} \, \mathrm{d}S \tag{8}$$

is obtained [11]. In Equation (8) S' is the area of a surface parallel to the inflow/outflow boundaries and $\mathbf{n}$ is the unit vector normal to the surface.

The behaviour of the flow is determined by the Reynolds number

$$Re = \frac{\bar{u} D_h}{\nu} \tag{9}$$

and is characterized by the friction factor

$$f = \frac{\alpha D_h}{\rho \bar{u}^2/2} \tag{10}$$

which is directly related to the mean pressure gradient α. The hydraulic diameter is defined as

$$D_h = \frac{2WH}{H + W/\sin\gamma} \tag{11}$$

The wall boundary condition utilized for the temperature is

$$t = t_w = \text{const} \tag{12}$$

At periodic boundaries, for wall boundary conditions of the first kind, the distribution of the dimensionless temperature

$$T = \frac{t - t_w}{t_b - t_w} \tag{13}$$

identically repeats itself from one corrugation cycle to the next [18]. Therefore, the anti-symmetric periodicity between corresponding points of a single module can be expressed as

$$\frac{t(L/2, y'', z) - t_w}{t_b(L/2) - t_w} = \frac{t(0, y', z) - t_w}{t_b(0) - t_w} \tag{14}$$

with reference to the boundaries S_1 and S_2 [11–13]. Equation (14) can be written in the form

$$t(L/2, y'', z) = \left[1 + \frac{t_b(L/2) - t_b(0)}{t_b(0) - t_w}\right] t(0, y', z) - \frac{t_b(L/2) - t_b(0)}{t_b(0) - t_w} t_w \tag{15}$$

In the above equations, t_b is the bulk temperature, which is usually defined as [11]

$$t_b = \frac{\int_{S'} |\mathbf{v} \cdot \mathbf{n}| t \, dS}{\int_{S'} |\mathbf{v} \cdot \mathbf{n}| \, dS} \tag{16}$$

Equation (15) contains two unknown quantities: the bulk temperature at inflow $t_b(0)$ and the difference between bulk temperatures at outflow and inflow $[t_b(L/2) - t_b(0)]$. In the solution process the value of the difference in bulk temperatures is imposed first, and then an iterative procedure is carried on until convergence is reached for a value of $t_b(0)$ which verifies the periodicity condition.

The average Nusselt number is defined as

$$Nu = \frac{h D_h}{k} \tag{17}$$

where

$$h = \frac{q}{S\overline{\Delta t}} \tag{18}$$

is the average heat transfer coefficient, S is the area of the heat transfer surface, q is the total rate of heat transfer and

$$\overline{\Delta t} = \Delta t_{\mathrm{lm}} = \frac{[t_{\mathrm{w}} - t_{\mathrm{b}}(L/2)] - [t_{\mathrm{w}} - t_{\mathrm{b}}(0)]}{\ln\{[t_{\mathrm{w}} - t_{\mathrm{b}}(L/2)]/[t_{\mathrm{w}} - t_{\mathrm{b}}(0)]\}} \tag{19}$$

is the logarithmic mean temperature difference.

2.2. Solution procedure

The momentum, continuity and energy equations are solved by the equal-order, finite element procedure based on the projection algorithm illustrated in Reference [19]. The anti-periodic boundary conditions are introduced as illustrated in detail in References [11–13]. The momentum and energy equations are discretized with respect to time, in a form that allows the selection of different time-integration schemes. At each time step a pseudo-velocity field is obtained first by neglecting the pressure gradients in the momentum equations. Then, by enforcing continuity on the pseudo-velocity field, a tentative pressure is estimated, and the momentum equations are solved for the corresponding tentative velocity field. Afterwards, continuity is enforced again to find pressure corrections. Pressure corrections are also used to find the velocity corrections that project the tentative velocity field onto a divergence-free space. Once the velocity field has been found, the energy equation is solved before moving to the next step.

The momentum and energy equations are dealt with as particular versions of a general transport equation, written in the time-discretized form

$$\rho\frac{\phi^{n+1} - \phi^{n}}{\Delta\vartheta} + \rho\mathbf{v}^{n}\cdot[\tau_v\nabla\phi^{n+1} + (1-\tau_v)\nabla\phi^{n}] = \Gamma[\tau_\Gamma\nabla^2\phi^{n+1} + (1-\tau_\Gamma)\nabla^2\phi^{n}] + \dot{s} \tag{20}$$

for a generic variable ϕ and a time step $\Delta\vartheta$. The properties ρ and Γ, and the volumetric source rate $\dot{s}$ are identified by inspection of the appropriate original equations for velocity components, pressure and temperature. The weighting factors τ_v and τ_Γ, both in the range from 0 to 1, allow the selection of different time-integration schemes. For example the Crank–Nicolson scheme, employed in this work, results from the choice: $\tau_v = \tau_\Gamma = 0.5$. The pressure equation and the pressure correction equation are also obtained from Equation (20), by assuming $\rho = 0$ and $\tau_\Gamma = \Gamma = 1$.

The space discretization of Equation (20) is based on the Bubnov–Galerkin method and the use of consistent mass and capacity matrices. The finite element procedure utilized for the solution of Equation (20) can be classified as a Bubnov–Galerkin Crank–Nicolson scheme with consistent mass and capacity matrices. In Reference [20], such a scheme has been identified as the most suitable choice for transient simulations with sufficiently refined meshes. In fact, the scheme is unconditionally stable and not affected by numerical diffusion, even if it presents a numerical dispersion that increases with the Courant number

$$Co = \frac{|v|\Delta\vartheta}{\Delta L} \tag{21}$$

referred to the time step and a characteristic dimension ΔL of the cell. Its order of accuracy, on a uniform mesh with linear elements, is $O(\Delta\vartheta^2, \Delta L^2)$, that is: second order with respect to both time integrations and space discretizations [20].

The systems of linear equations, arising at each time step from the discretization process, are solved by means of iterative algorithms. The conjugate gradient squared (CGS) method is used to solve the discretized momentum and energy equations, while the modified conjugate gradient method (MCG) is used to solve the symmetric systems obtained from the discretization of the Poisson equations. In both cases, preconditioned matrices are obtained from an incomplete LU decomposition (ILU).

3. RESULTS AND DISCUSSION

As already pointed out, all previous studies on wavy channels agree about enhancement effects connected with increasing the space ratio H/L and the corrugation angle β, and decreasing the aspect ratio W/H [12–17]. Since it can be assumed that the same conclusions also apply to trapezoidal channels, this paper only investigates the effect of corner angle variations. In accordance with References [12, 13], the values $H/L = 0.15$, $\beta = 20^\circ$ and $W/H = 1$ have thus been kept constant, while the values $\gamma = 90$, 75, 60 and 45° have been adopted for the corner angle. Calculations have been carried out for laminar convection of air ($Pr = 0.72$), in a range of Reynolds numbers from $Re = 100$ to values above the critical Reynolds number Re_{cr} associated with the onset of self-sustained flow oscillations.

By imposing $W/H = 1$ in Equation (11), we easily arrive at the relationship

$$\frac{H}{D_h} = \frac{1 + \operatorname{sen}\gamma}{2\operatorname{sen}\gamma} \tag{22}$$

The use of the hydraulic diameter as the reference length yields the cross-sectional shapes represented in Figure 2. In particular, the value $\gamma = 90^\circ$ leads to a square section, while the value $\gamma = 45^\circ$ leads to an isosceles triangular section.

Cross-sections of grids used in the discretization process are illustrated in Figure 3, where the $\gamma = 75$ and 45° geometries are reported as an example. Structured meshes have been utilized for rectangular and trapezoidal sections, while block-structured meshes have been employed for triangular sections. In both cases, spacings are finer near the walls. The final three-dimensional meshes have been obtained by extruding, deforming and cutting into

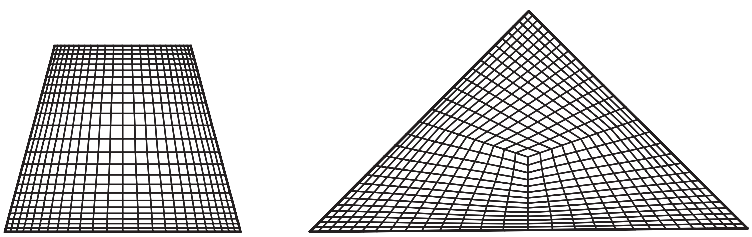

Figure 3. Cross-sections of grids used in the discretization process: $\gamma = 75^\circ$ (left) and $\gamma = 45^\circ$ (right).

Table I. Friction factors and Nusselt numbers for fully developed velocity and temperature fields in straight trapezoidal channels for $W/H = 1$ and different corner angles.

γ (°)	$(fRe)_0$		Nu_0	
	Reference [3]	Present	Reference [3]	Present
90	57.00	57.04	2.96	2.97
75	56.72	56.62	2.89	2.90
60	55.44	55.43	2.70	2.71
45	52.64	52.71	2.34	2.34

eight-node (brick) elements the two-dimensional meshes. The resulting brick elements have been spaced more closely near the inflow/outflow sections.

The calculations concern steady- and unsteady-state solutions that have been obtained from pseudo-transient, or transient, simulations, respectively. When the flow character changed from steady to oscillatory, space-averaged parameters were further averaged over a period Θ yielding single representative values

$$\langle\varphi\rangle = \frac{1}{\Theta}\int_{\vartheta}^{\vartheta+\Theta} \varphi(\vartheta)\,\mathrm{d}\vartheta \tag{23}$$

with $\varphi = f$ or Nu. To lighten the notation, the symbol $\langle\,\rangle$ has always been omitted, except when referring to time-averaged velocity vectors.

Grid independence has been established on the basis of preliminary calculations, in which the distance between grid points has been progressively reduced by 30% from one simulation to another. When a further decrease led to a change in the average Nusselt numbers smaller than 1%, the results were considered to be grid-independent. In the final simulations the number of nodal points, and the corresponding number of elements, varied from 30 625 ($=25\times25\times49$) nodal points and 27 648 elements for structured meshes, to 30 919 ($=631\times49$) nodal points and 28 224 elements for block-structured meshes. Time-step independence has also been established on the basis of preliminary calculations in which the dimensionless time step $\Delta\theta = \bar{u}\Delta\vartheta/L$ has been progressively reduced by 30% from one simulation to another. When a further decrease led to a change in the average Nusselt numbers smaller than 1%, the results were considered to be independent of the time step. In the final simulations, a Crank–Nicolson scheme with a dimensionless time step equal to 0.01 has been used for transient solutions, and a fully implicit scheme with a dimensionless time step equal to 0.02 has been used for steady-state solutions.

The reliability of the calculation procedure described in previous sections had already been demonstrated [11–13]. However, the accuracy has been assessed once again here by imposing periodicity conditions on small portions of straight trapezoidal channels characterized by different corner angles. In this way, results concerning friction factors and Nusselt numbers for fully developed velocity and temperature fields in straight channels have been obtained. As shown in Table I, the numerical results for $W/H = 1$ and $\gamma = 90$, 75, 60, and 45° are independent of the Reynolds and Prandtl numbers and agree to the third digit with the analytical solutions proposed in Reference [3]. It is interesting to note that, in straight trapezoidal channels, friction factors and Nusselt numbers decrease with decreasing corner angles. On

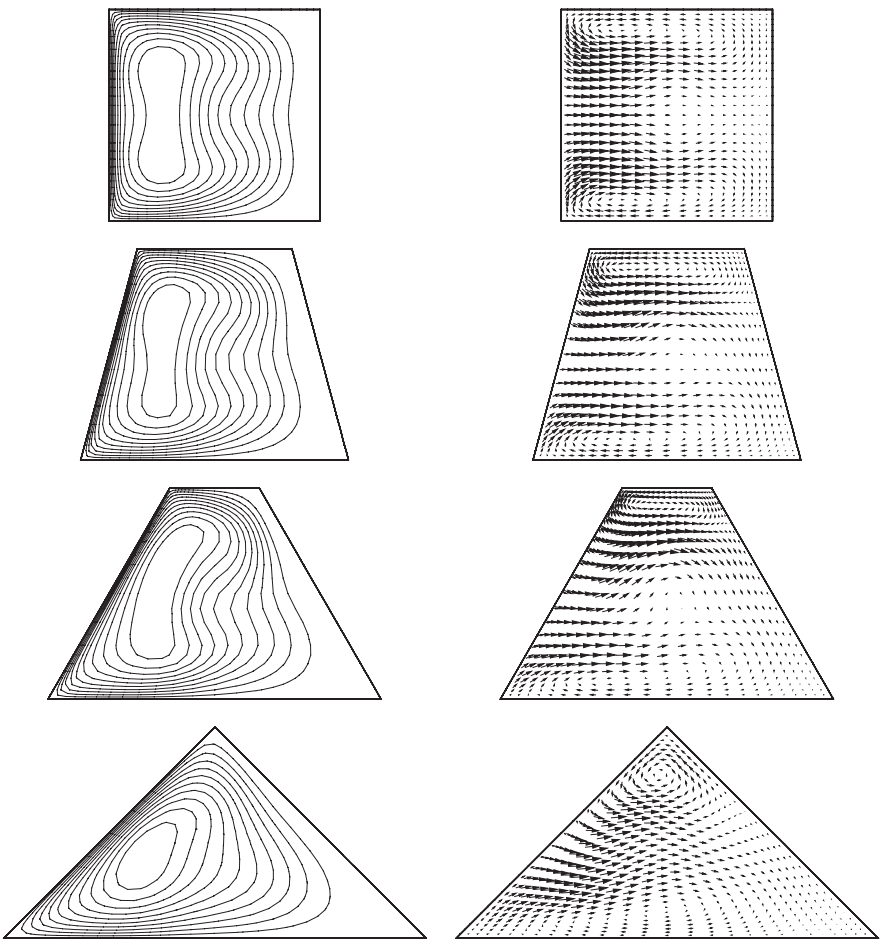

Figure 4. Contours of streamwise velocity components and transverse velocity vectors at inlet sections of modules for $Re = 200$.

the other hand, the conclusions reached for straight channels, where longitudinal vortices and transverse flow oscillations do not occur, cannot be assumed to hold good also for wavy channels, where longitudinal vortices and transverse flow oscillations are expected.

3.1. Influence of longitudinal vortices

In all channels, and in the whole range of Reynolds numbers investigated, two longitudinal counter-rotating vortices have been found close to the parallel walls. Contours of streamwise velocity components u and transverse velocity vectors are shown in Figure 4 for $Re = 200$, a lower than critical value for all the channels considered. In this figure, reference is made to the inlet section ($x = 0$) where the inner wall of the bend appears on the left. As can be seen, the centrifugal force due to the curvature pushes the peak of the axial velocity from the inner bend towards the outer wall. In the vicinity of upper and lower walls, where streamwise

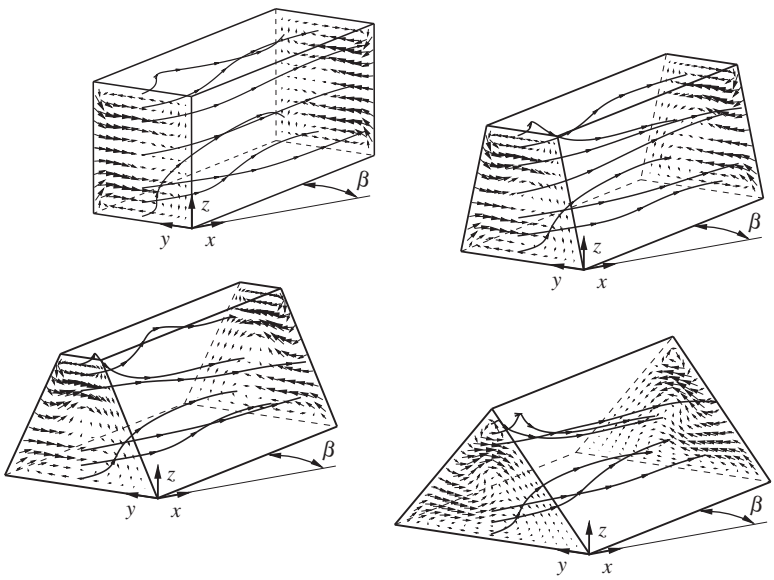

Figure 5. Trajectories and transverse velocity vectors at inlet/outlet sections of modules for $Re = 200$.

velocities are limited by viscous forces, this produces the secondary flows visualized by the transverse velocity vectors.

Trajectories and transverse velocity vectors at inlet/outlet sections of a module are illustrated in Figure 5, where the development of the two longitudinal counter-rotating vortices is clearly visible. Angular velocities have opposite signs on inlet and outlet sections of each module. Magnitudes of rotational velocities are the largest at inlet/outlet sections of the module and tend to zero in one intermediate section.

Secondary flows, associated with longitudinal vortices, move fluid from the walls to the centre and, thus, have a beneficial effect on the distribution of heat fluxes q^n. Wall distributions of heat fluxes are shown in Figure 6, where lighter tones are associated with higher values of the dimensionless parameter $q''/q''_{\max}$. As can be seen, secondary flows connected with longitudinal vortices leave clear traces in the heat flux distribution.

3.2. Influence of flow oscillations

Until flows remain steady (i.e. for $Re < Re_{\mathrm{cr}}$), transverse vortices are confined to recirculation zones where little fluid enters. Therefore, the growth of recirculation zones with the Reynolds number increases pressure losses by diminishing the areas of main flow passages, but does not contribute to the enhancement of heat transfer [8, 12, 13]. At $Re > Re_{\mathrm{cr}}$, transverse vortices start detaching periodically and moving downstream. This process transports fresh fluid from the walls to the core, enhancing rates of energy transfer. The value of the critical Reynolds number depends on the geometrical configuration. Its direct calculation is an almost impossible task because the transients become longer and longer as one approaches the critical point and the amplitude of the oscillations tends to zero. Thus the results of Table II refer to a

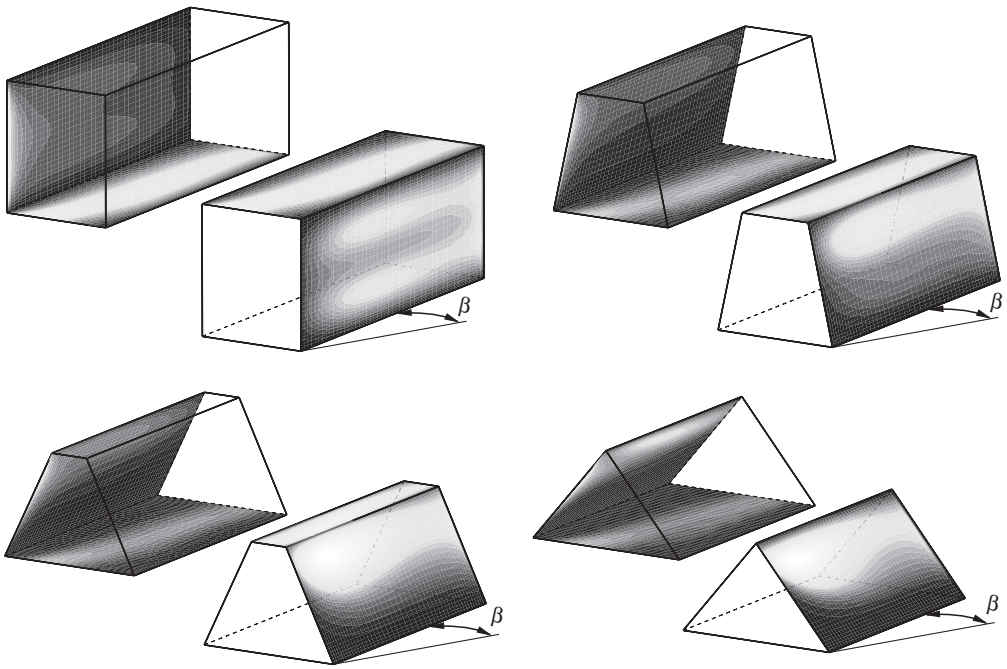

Figure 6. Distributions of dimensionless heat fluxes $q''/q''_{\max}$ at $Re = 200$. Lighter tones are associated with higher values.

Table II. Wavy trapezoidal channels with $H/L = 0.15$, $\beta = 20°$, $W/H = 1$ and different corner angles γ: approximate values of the critical Reynolds number (Re_{cr}), and dominant frequencies (St) of the oscillations of the space-averaged Nusselt number at $Re = 270$.

γ (°)	45	60	75	90
Re_{cr}	250	265	230	240
St	0.56	0.52	0.11	0.12

condition slightly above the critical, and the values reported have been found by a trial-and-error procedure.

With reference to Figure 7, let us consider the projections of differences $\mathbf{v} - \langle \mathbf{v} \rangle$ between instantaneous and time-averaged velocities on the horizontal mid-planes of the investigated channels at $Re = 270$, a higher than critical value for all the channels considered. From the instantaneous representations it does appear that lateral walls are washed by transverse vortices travelling downstream. The highest intensities of transverse vortices at $\gamma = 90$ and 75° correspond to the lowest values of the critical Reynolds number, while the lowest intensities at $\gamma = 60$ and 45° correspond to the highest value of the critical Reynolds number. In fact, the intensity of transverse vortices increases with the Reynolds number for $Re > Re_{cr}$, since at Re_{cr} the flow starts a transition towards turbulence.

The time behaviour of the Nusselt number at $Re = 270$ is illustrated in Figure 8 for all the ducts considered. In this figure, the variations of the Nusselt number with the

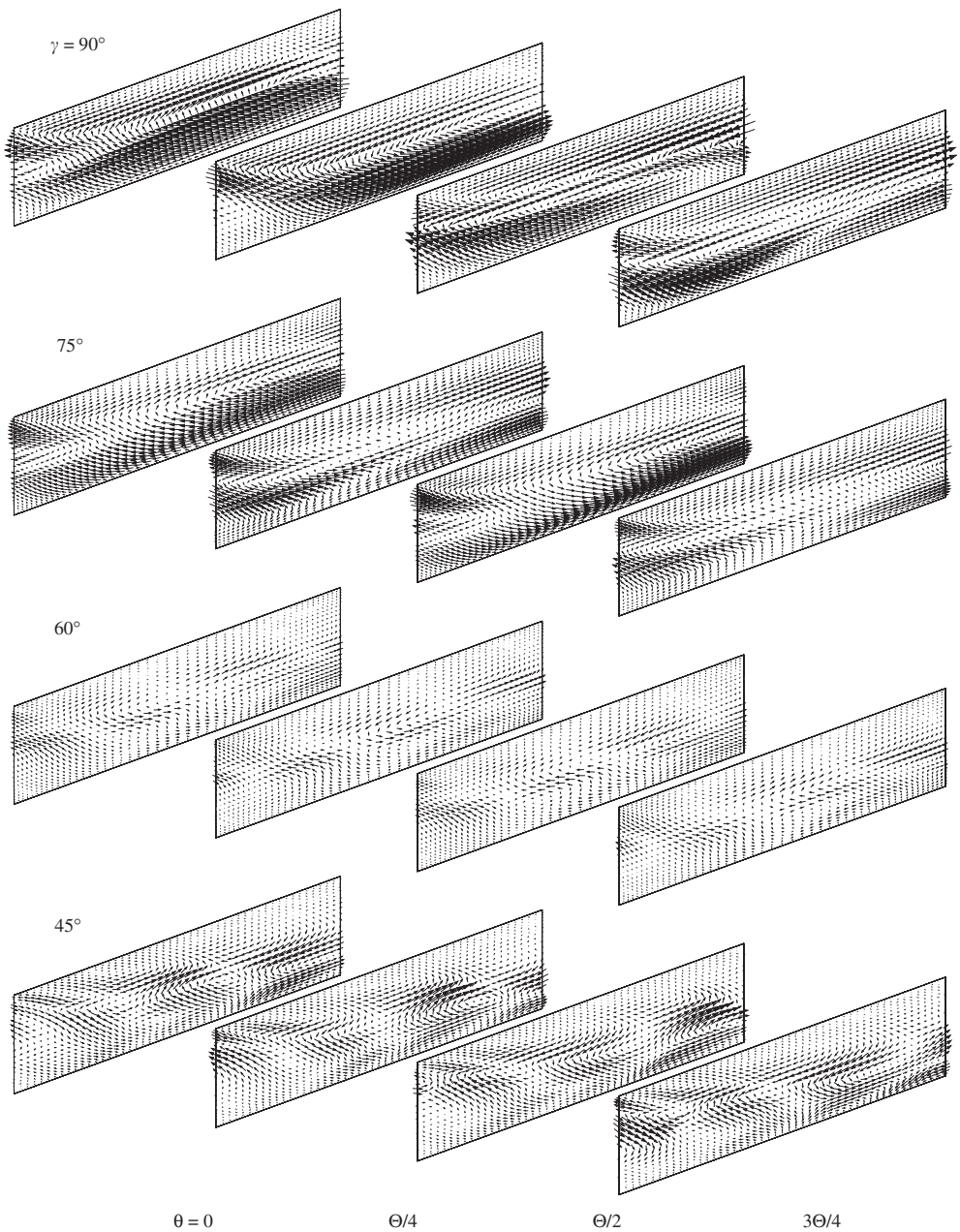

Figure 7. Wavy trapezoidal ducts at $Re = 270$: differences between instantaneous and time-averaged velocity vectors in the vertical mid-plane at $\Theta/4$ intervals.

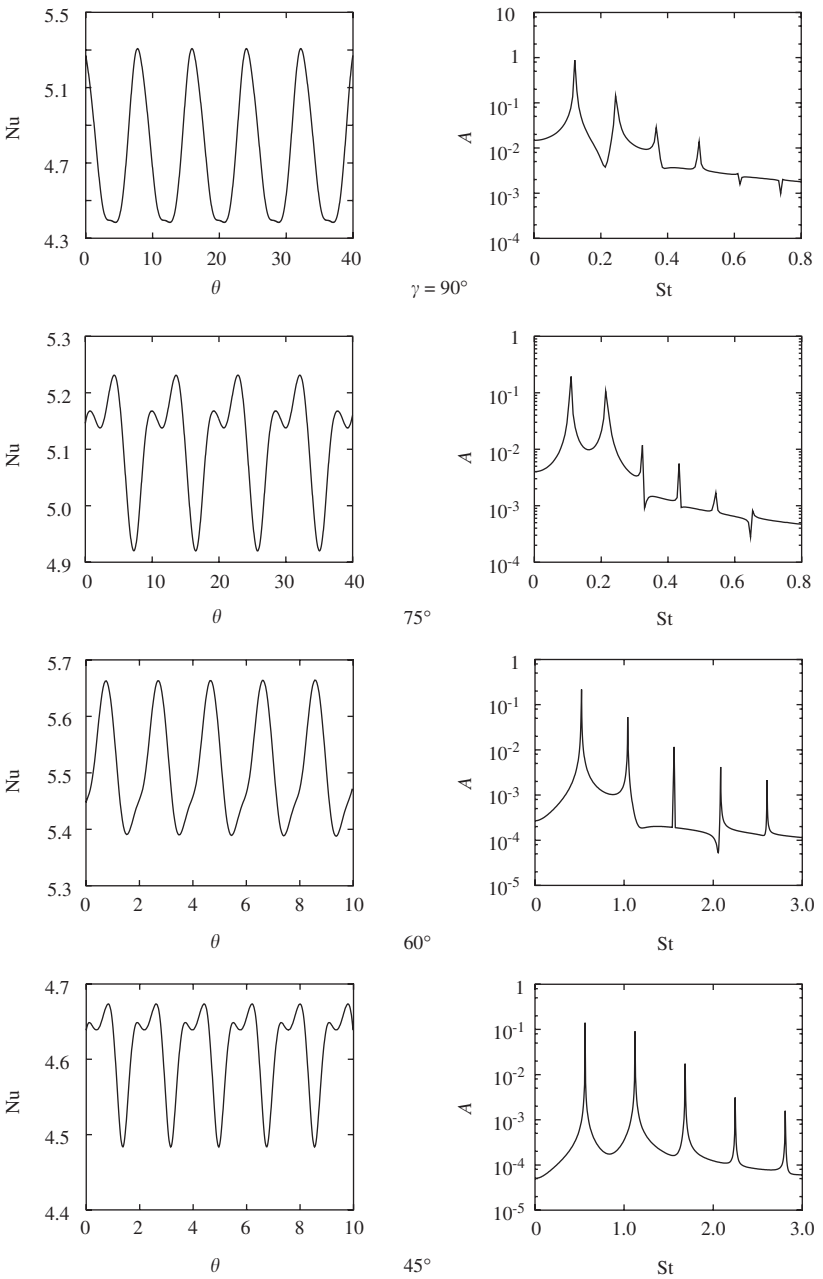

Figure 8. Wavy trapezoidal ducts at $Re = 270$: time behaviour of the space-averaged Nusselt number (left), and corresponding power density spectra of peak-to-peak amplitudes of its oscillations (right).

dimensionless time

$$\theta = \frac{\vartheta \bar{u}}{D_h} \tag{24}$$

are plotted on the left, while the corresponding spectra of the peak-to-peak amplitudes A of its oscillations are plotted on the right as a function of the dimensionless frequency (the Strouhal number)

$$St = \frac{D_h}{\bar{u}\Theta} \tag{25}$$

As expected, all Nu vs θ representations indicate time-periodic behaviour at $Re = 270$. Correspondingly, the fast Fourier transform shows dominant frequencies whose dimensionless values, i.e. Strouhal numbers, seem to change according to a Feigenbaun-like scenario of transition to turbulence. The route described by Feigenbaun involves a series of successive frequency-halving bifurcations that are brought about by the increase of the Reynolds number [21]. In the Fourier space, these inverse cascades first yield a quite distributed spectrum over a broad frequency range and, at the end, a transition to chaos. In the flows investigated here, the increase of corner angle plays a role that is similar to the increase of the Reynolds number in constant geometries ducts. As shown in Table II the highest values of the Strouhal number correspond to the lowest values of corner angle ($\gamma = 45$ and $60°$), while the lowest values of the Strouhal number correspond to the highest values of corner angle ($\gamma = 75$ and $90°$). In particular, for $\gamma = 75°$ we have the lowest values of both the Strouhal number ($St = 0.11$) and the critical Reynolds number ($Re_{cr} = 230$). Furthermore, numerical calculations, not illustrated here, have shown that the $\gamma = 75°$ geometry is the first to undergo a transition to chaos (around $Re = 280$).

3.3. *Quantitative comparisons*

The momentum and heat transfer characteristics of wavy ducts can be described in terms of average Nusselt numbers and apparent friction factors. In Figure 9, the values of f and Nu pertaining to wavy ducts with trapezoidal cross-sections have been divided by the values of f_0 and Nu_0 pertaining to the fully developed regions of straight trapezoidal ducts with the same cross-sections. For a given Reynolds number, these amplification factors increase with decreasing values of the corner angle, but level out around $\gamma = 60°$. For a given corner angle, amplification factors always increase with the Reynolds number. In correspondence with the critical value of the Reynolds number the slopes of the f/f_0 and Nu/Nu_0 vs Re curves increase because of the onset of transverse vortices. The changes in slope are more pronounced in the $\gamma = 90$ and $75°$ ducts, where the intensities of transverse vortices are higher, than in the $\gamma = 60$ and $45°$ ducts, where the intensities of transverse vortices are lower.

In Figure 10, the values of $f\mathrm{Re}$ and Nu have been compared for the different cross-sections. As can be seen, friction factors and Nusselt numbers first increase with decreasing corner angles, but then start to decrease around $\gamma = 60°$. For straight channels, on the contrary, the results of Table I demonstrate that both friction factors and Nusselt numbers decrease monotonically with decreasing corner angles. Thus the conclusions reached for straight trapezoidal channels, where longitudinal vortices and transverse flow oscillations are absent, do not apply to wavy trapezoidal channels where longitudinal vortices and transverse flow oscillations play a very important role.

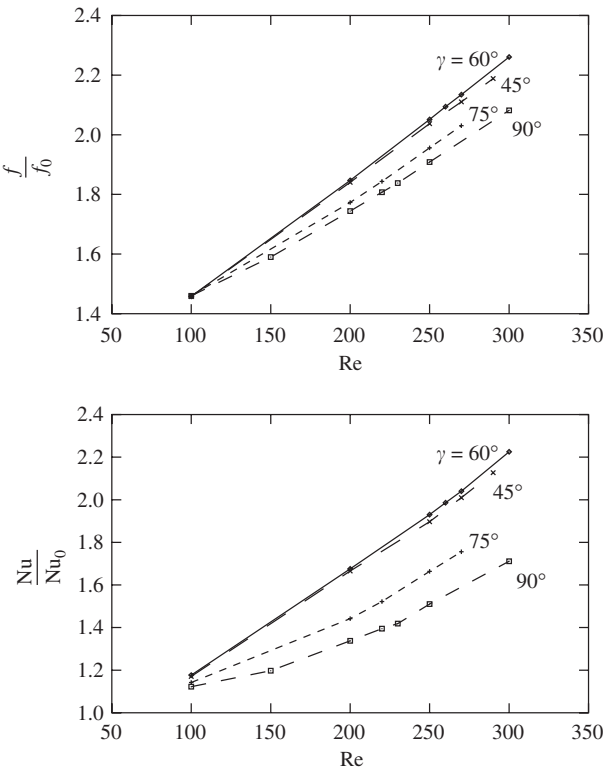

Figure 9. Apparent friction factors and average Nusselt numbers in wavy trapezoidal ducts, normalized with corresponding values for straight trapezoidal ducts with the same cross-section.

3.4. Performance evaluation

In boundary layer flows, the momentum and heat transfer characteristics are related by the Chilton–Colburn analogy, which can be written in the form

$$\varepsilon = \frac{j}{f} = \frac{Nu}{RePr^{1/3}} \frac{1}{f} = \text{const} \tag{26}$$

where j is the Colburn factor for heat transfer, and ε can be interpreted as a goodness factor. This analogy is strictly valid for boundary layer flows over a flat plate but, by adjusting the value of the constant, the analogy can still be applied to other non-recirculating flows. In recirculating flows, such as the ones occurring in wavy ducts with trapezoidal cross-sections, the Chilton–Colburn analogy does not hold good, but $\varepsilon/\varepsilon_0$ and ε can still be used in performance comparisons of the kind reported in Figure 11. Once again the subscript 0 indicates that reference is made to a straight duct with the same cross-section.

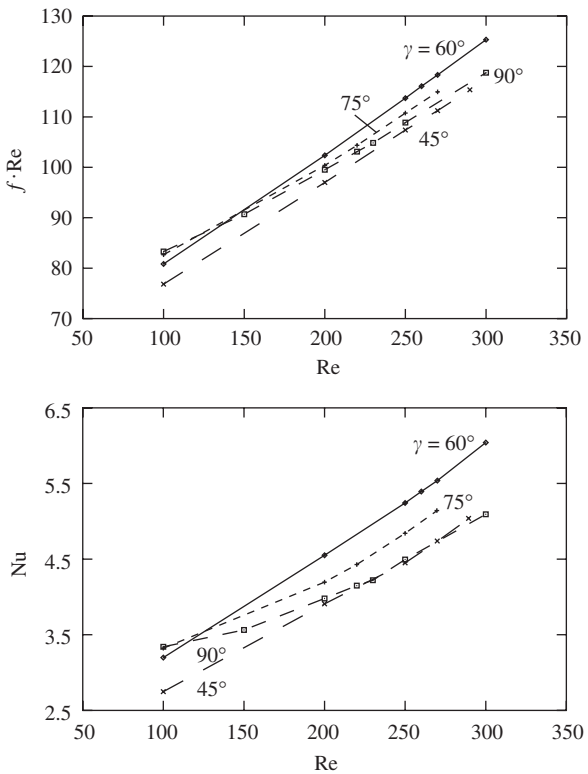

Figure 10. Apparent friction factors and average Nusselt numbers in wavy trapezoidal ducts.

4. CONCLUSIONS

The effect of corner angle variations has been investigated with respect to the enhancement of convection heat transfer in the fully developed region of three-dimensional wavy channels with trapezoidal cross-sections. The discretization has been based on a finite element procedure utilizing a Bubnov–Galerkin Crank–Nicolson scheme with consistent mass and capacity matrices. Velocity and temperature fields obtained from the numerical simulations reveal the existence of longitudinal vortices close to the parallel surfaces. These vortices enhance the transport of energy by mixing fluid near walls with fluid in the central part of the duct. Furthermore, when the flow and temperature fields become unsteady, above a critical value of the Reynolds number, a new convective heat transfer mechanism appears: the periodic washing of the inclined walls by travelling transverse vortices.

Quantitative results have been obtained for Nusselt numbers, apparent friction factors and goodness factors. For a given Reynolds number, Nusselt numbers and friction factors increase initially with the decrease of the corner angle γ from 90 to 60°, but then level out around $\gamma = 60°$. For a given corner angle, Nusselt numbers and friction factors always increase with the Reynolds number. Furthermore, in correspondence with the critical value of the Reynolds

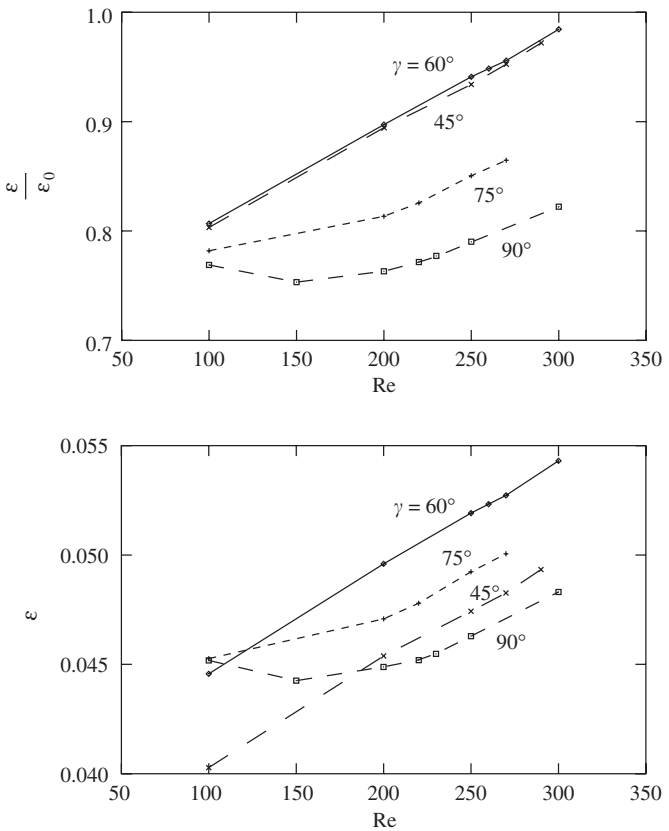

Figure 11. Goodness factors in wavy trapezoidal ducts. Subscript '0' indicates reference to a straight duct with the same cross-section.

number, the slopes of the friction factor and Nusselt vs *Re* curves increase because of the onset of time-periodic flow oscillations.

REFERENCES

1. Shah RK, London AL. Laminar flow forced convection in ducts. *Advances in Heat Transfer* (*Suppl.* 1). Academic Press: New York, 1978.
2. Shah RK, Bhatti MS. Laminar convective heat transfer in ducts. In *Handbook of Single-Phase Convective Heat Transfer*, Kakac S, Shah RK, Aung A (eds), Chapter 3. Wiley: New York, 1987.
3. Sadasivam R, Manglik RM, Jog Ma. Fully developed convection through trapezoidal and hexagonal ducts. *International Journal of Heat and Mass Transfer* 1999; **42**:4321–4331.
4. Bhatti MS, Shah RK. Turbulent and transition flow convective heat transfer in ducts. In *Handbook of Single-Phase Convective Heat Transfer*, Kakac S, Shah RK, Aung A (eds), Chapter 4. Wiley: New York, 1987.
5. Farhanieh B, Sundén B. Three-dimensional laminar flow and heat transfer in the entrance region of trapezoidal ducts. *International Journal for Numerical Methods in Fluids* 1991; **13**:537–556.
6. Nakayama A, Chow WL, Sharma D. Calculation of fully turbulent flow in ducts of arbitrary cross-section. *Journal of Fluid Mechanics* 1983; **128**:199–217.
7. Rokni M, Sundén B. Numerical investigation of turbulent forced convection in a duct with a trapezoidal cross-section. In *Advances in Engineering Heat Transfer*, Sundén B, Blums E, Zukauskas A (eds). Computational Mechanics Publications: Southampton, 1995; 321–331.

8. Fiebig M. Vortices: tools to influence heat transfer—recent developments. In *Proceedings of the 2nd European Thermal-Sciences and 14th UIT National Heat Transfer Conference*, *Rome*. Celata GP, Di Marco P, Mariani A (eds), vol. 1. Edizioni ETS: Pisa, 1996; 41–56.
9. Asako Y, Faghri M, Sundén B. Laminar flow and heat transfer characteristics of a wavy duct with a trapezoidal cross section for heat exchanger application. In *Proceedings of the 2nd European Thermal-Sciences and 14th UIT National Heat Transfer Conference*, *Rome*. Celata GP, Di Marco P, Mariani A (eds), vol. 2. Edizioni ETS: Pisa, 1996; 1097–1104.
10. Asako Y, Faghri M, Sundén B. Three-dimensional laminar forced convection characteristics of wavy ducts with trapezoidal cross section for plate-fin heat exchanger. In *Computer Simulations in Compact Heat Exchangers*, Sundén B, Faghri M (eds), vol. 1. Computational Mechanics Publication: Southampton, 1998; 49–75.
11. Nonino C, Comini G. Finite-element analysis of convection problems in spatially periodic domains. *Numerical Heat Transfer*, *Part B* 1998; **34**:361–378.
12. Comini G, Nonino C, Savino S. Effect of space ratio and corrugation angle on convection enhancement in wavy channels. *International Journal of Numerical Methods for Heat and Fluid Flow* 2003; **13**:500–519.
13. Comini G, Nonino C, Savino S. Effect of aspect ratio on convection enhancement in wavy channels. *Numerical Heat Transfer*, *Part A* 2003; **44**:21–37.
14. Goldstein L Jr, Sparrow EM. Heat/mass transfer characteristics for flow in a corrugated wall channel. *Journal of Heat Transfer* 1977; **99**:187–195.
15. O'Brien JE, Sparrow EM. Corrugated-duct heat transfer, pressure drop, and flow visualization. *Journal of Heat Transfer* 1982; **104**:410–416.
16. Sparrow EM, Comb JW. Effect of interwall spacing and fluid flow inlet conditions on a corrugated wall heat exchanger. *International Journal of Heat and Mass Transfer* 1983; **26**:993–1005.
17. Ali MM, Ramadhyani S. Experiments on convective heat transfer in corrugated channels. *Experimental Heat Transfer* 1992; **5**:175–193.
18. Kelkar KM, Patankar SV. Numerical prediction of periodically fully developed flow and heat transfer in a parallel plate channel with staggered fins. *Journal of Heat Transfer* 1987; **109**:25–30.
19. Nonino C, Comini G. An equal order pressure–velocity algorithm for incompressible thermal flows—Part 1: formulation. *Numerical Heat Transfer*, *Part B* 1997; **32**:1–15.
20. Comini G, Manzan M, Nonino C. Analysis of finite element schemes for convection-type problems. *International Journal for Numerical Methods in Fluids* 1995; **20**:443–458.
21. Feigenbaum MJ. Quantitative universality for a class of nonlinear transformations. *Journal of Statistical Physics* 1978; **19**:24–52.

